Evaluation of different measures of functional connectivity using a neural mass model

Olivier David,[a],* Diego Cosmelli,[b] and Karl J. Friston[a]

[a] Functional Imaging Laboratory, Wellcome Department of Imaging Neuroscience, London WC1N 3BG, UK
[b] CNRS UPR 640 Neurosciences Cognitives et Imagerie Cérébrale, Hôpital de la Salpêtrière, 75651 Paris Cedex 13, France

We use a neural mass model to address some important issues in characterising functional integration among remote cortical areas using magnetoencephalography or electroencephalography (MEG or EEG). In a previous paper [Neuroimage (in press)], we showed how the coupling among cortical areas can modulate the MEG or EEG spectrum and synchronise oscillatory dynamics. In this work, we exploit the model further by evaluating different measures of statistical dependencies (i.e., functional connectivity) among MEG or EEG signals that are mediated by neuronal coupling. We have examined linear and nonlinear methods, including phase synchronisation. Our results show that each method can detect coupling but with different sensitivity profiles that depended on (i) the frequency specificity of the interaction (broad vs. narrow band) and (ii) the nature of the coupling (linear vs. nonlinear).

Our analyses suggest that methods based on the concept of generalised synchronisation are the most sensitive when interactions encompass different frequencies (broadband analyses). In the context of narrow-band analyses, mutual information was found to be the most sensitive way to disclose frequency-specific couplings. Measures based on generalised synchronisation and phase synchronisation are the most sensitive to nonlinear coupling. These different sensitivity profiles mean that the choice of coupling measures can have dramatic effects on the cortical networks identified. We illustrate this using a single-subject MEG study of binocular rivalry and highlight the greater recovery of statistical dependencies among cortical areas in the beta band when mutual information is used.

© 2003 Elsevier Inc. All rights reserved.

Keywords: Neural mass model; Synchronisation; Functional connectivity

Introduction

The complicated nature of brain connectivity, composed of local networks interconnected by long range pathways, is well known and is the principal determinant of its functional organisa-tion (Abeles, 1991; Sporns et al., 2000). The ensuing architecture means that the brain can be understood as a dynamical system, comprising a huge number of state variables generating many distinct and metastable states. This metastability endows the brain with a characteristic lability, that is, sensitivity to change, which arises from a capacity to self-organise through modulating its internal structure (Friston, 2000). This modulation is context dependent, occurs over different time scales and can be transient (e.g., changes of connectivity due to attention modulation) or enduring (e.g., somatotopic reorganisation due to limb amputation).

Integration or functional connectivity is usually inferred by statistical dependencies among signals in coupled neuronal systems. It is possible to analyse these dependencies using noninvasive macroscopic measures such as magnetoencephalography (MEG) (Hamalainen et al., 1993) and electroencephalography (EEG) (Nunez, 1981). However, the variability of MEG or EEG signals and our incomplete understanding of the neuronal processes generating them make their analysis particularly difficult. Indeed characterising dynamic patterns is tricky due to the intrinsic complexity and nonlinearity of the underlying neuronal processes (Abarbanel and Rabinovich, 2001).

There is an uncertain consensus about the best method to characterise neuronal couplings with MEG or EEG. Interactions can be synchronous or asynchronous, linear or nonlinear and so forth, engendering many different types of synchronisation, that is, a common behaviour of at least one property of MEG or EEG generators (Boccaletti et al., 2002; Pikovsky et al., 2001). This may be why different dependency measures appear in the MEG or EEG literature: these include linear (cross-correlation, coherence; Clifford Carter, 1987) or nonlinear (mutual information; Roulston, 1999), nonlinear correlation (Pijn et al., 1992), mutual dimension (Buzuk et al., 1994), nonlinear interdependencies or generalised synchronisation (Arnhold et al., 1999; Schiff et al., 1996; Stam and van Dijk, 2002; Stam et al., 2003), neural complexity (Tononi et al., 1994)) or are based upon the quantification of phase locking of oscillations (phase synchronisation; Lachaux et al., 1999; Tass et al., 1998). This battery of measures has been assembled during the last decade, making research in this area exciting but quite confusing. Recently, an attempt has been made to evaluate the performance of some of these measures in a case study of EEG signals (Quian Quiroga et al., 2002). The authors conclude that,

---

with the exception of mutual information, all these measures give qualitatively equivalent results, with nonlinear measures being more sensitive.

The aim of this paper was to compare a set of commonly employed measures to assess their relative efficacy for detecting neuronal coupling. Our strategy was to use simulated neuronal processes in which we could manipulate the coupling between two cortical areas. Using surrogate or null data, we determined the null distribution of each measure to enable its sensitivity to be evaluated. This represents an assessment in terms of each measure's ability to detect statistical dependencies among remote neurophysiological indices. These dependencies define, operationally, "functional connectivity". In this paper, we focus on measuring functional connectivity in continuous neuronal time series. Note that this does not constitute an analysis of "effective connectivity" (the influence one neuronal system exerts over another): We are not interested, here, in the mechanism of the coupling or indeed how the dependencies are expressed (e.g., linear vs. nonlinear). We simply want to establish whether dependencies exist and find their most sensitive measure. In a later paper, we will deal with similar issues in the context of transient responses and induced oscillations.

The measures considered in this work were linear (cross-correlation function or first-order cumulant) and nonlinear. The nonlinear measures represented static (mutual information) and dynamic measures. The latter were phase synchronisation and one based on the concept of generalised synchronisation. We anticipated that measures encompassing nonlinear and dynamic dependencies would supervene over linear and static metrics, given the way neuronal interactions are mediated. However, each estimator has its own bias and variance that may be important when dealing with finite time series.

In this paper, we use a model of MEG or EEG signals in which we changed the coupling strength between two cortical areas. This allowed us to assess the sensitivity of various interaction measures using oscillatory signals that simulate normal, ongoing MEG or EEG activity. The principal characteristics of the model have been presented in a companion paper (David and Friston, in press) and are described only briefly here. Our model is a generalisation, to multiple neuronal populations, of the Jansen model (Jansen and Rit, 1995) operating in its oscillatory regime. The Jansen model was based on previous work in the 1970s (Freeman, 1978; Lopes da Silva et al., 1974) modelling EEG and visual-evoked potentials. Recently, it has been modified to generate epileptic activity (Wendling et al., 2000). A specific characteristic of our model is that it exhibits oscillatory behaviours that are driven by stochastic noise. Our model generates more complicated activity than the Jansen model because different neuronal populations are endowed with different kinetics. Our generalised model was designed to assess the consequences of coupling changes in the context of oscillatory dynamics. This complements the modelling initiative in (Wendling et al., 2001) for epileptic activity.

Modelled cortical areas are composed of interacting inhibitory and excitatory populations with slow and fast kinetics. Two operations are used to integrate the model: a spike density-to-membrane potential conversion, which depends linearly upon neuronal kinetics; and the inverse conversion, which is considered instantaneous and nonlinear (a sigmoid function). Different areas are coupled by excitatory connections whose strength is set by a coupling parameter. We have shown, qualitatively, that coupling areas results in a phase locking of their activities. The purpose of

using this model here is to demonstrate that the sensitivity profile of each measure differs and that a complete description of interactions calls for the use of several approaches.

In the first section, we introduce the different measures of interdependencies among MEG or EEG signals that are considered in subsequent sections. Then we use our neural mass model to evaluate their sensitivity to coupling in the context of nonlinear interactions. Finally, we show how findings obtained from simulations translate using real MEG data from a binocular rivalry study.

Dependency measures

Consider two discrete univariate time series x_n and y_n, $n = 1,\dots$, N measured simultaneously. A dependency measure quantifies relationships between these time series, induced by interactions at the level of the generating processes. Each dependency measure has particular characteristics and we divide them into three groups: linear, nonlinear and phase related. The linear measures are fast but insensitive to nonlinear coupling in contrast to nonlinear measures. The phase-related measures are nonlinear but consider that the state variables of interest are the instantaneous phases $\Phi_{x,y}$ of oscillations instead of their instantaneous amplitudes x,y.

Linear measures

The most commonly used measure of first-order interactions between two time series x and y is the linear cross-correlation function $c_{xy}(l)$ defined as

$$c_{xy}(l) = \left\langle \left(\frac{x_i - \bar{x}}{\sigma_x}\right)\left(\frac{y_{i+l} - \bar{y}}{\sigma_y}\right) \right\rangle_i \tag{1}$$

where $\bar{x}$ and σ_x are the mean and standard deviation of x, similarly for y, and l is a time lag. The absolute value of c_{xy} ranges from 0 (no interaction) to 1 (x and y are proportional).

The coherence function $\Gamma_{xy}(\omega)$ is the normalised value of the cross-spectrum $C_{xy}(\omega)$ defined as the Fourier transform of the cross-correlation function $c_{xy}(l)$:

$$\Gamma_{xy}(\omega) = \frac{|C_{xy}(\omega)|}{\sqrt{|C_{xx}(\omega)||C_{yy}(\omega)|}} \tag{2}$$

where ω is the discrete frequency. $\Gamma_{xy}(\omega)$ takes its values between 0 and 1. It has been shown that coherence is useful for quantifying long-range interactions in the EEG (Bressler, 1995; Gross et al., 2001; Nunez et al., 1997). However, as the information contained in the cross-correlation function and coherence function is identical, we restrict our analyses to the cross-correlation function. We define our linear measure of interactions as $\max_l(c_{xy})$ and refer to it as the cross-correlation.

Nonlinear measures

Mutual information

The measure of mutual information (MI) between two random variables X and Y is based upon concepts from information theory. It indicates the amount of information in X, given that Y is known and vice versa. If the random variable X is partitioned into I bins,

then a probability p_i^X can be assigned to each possible outcome $X_i (i = 1, \ldots, I)$: $p_i^X = n_i^X/N$ where n_i^X is the number of occurrences of X_i after N samples. The Shannon entropy of X is defined as

$$H(X) = -\sum_{i=1}^{I} p_i^X \ln p_i^X. \tag{3}$$

The estimation of $H(X)$ is biased when some bins contain no points ($p_i^X = 0$). This occurs with finite time series, leading to an underestimate of the entropy. The systematic bias can be compensated for by estimating the errors introduced by the partitioning into bins. The corrected entropy H^∞ (Roulston, 1999) is then defined as:

$$H^\infty(X) = H(X) + \frac{b_X - 1}{2N} \tag{4}$$

where b_X is the number of states for which $p_i^X \neq 0$. Similarly, the joint entropy between X and Y is equal to

$$H(X, Y) = -\sum_{i,j} p_{ij}^{XY} \ln p_{ij}^{XY}. \tag{5}$$

where p_{ij}^{xy} is the joint probability of $X = X_i$ and $Y = Y_j$. Finally, the mutual information between X and Y is defined as

$$\text{MI}(X, Y) = H(X) + H(Y) - H(X, Y) \tag{6}$$

and its bias corrected expression MI^∞ (Roulston, 1999) is

$$\text{MI}^\infty(X, Y) = \text{MI}(X, Y) + \frac{b_X + b_Y - b_{XY} - 1}{2N} \tag{7}$$

where b_X, b_Y and b_{XY} are the number of bins containing points. In the following, the mutual information is bias corrected and normalised by dividing it by $\ln(I)$.

The mutual information quantifies the statistical dependencies between the two variables X and Y, with no assumption about the form of their respective densities and implicitly their generating processes, which can be linear or nonlinear. Unless some form of temporal embedding is used (Quian Quiroga et al., 2002), this sort of measure is only sensitive to static nonlinear dependencies.

Generalised synchronisation

The broad concept of generalised synchronisation was introduced in 1995 (Rulkov et al., 1995). By definition, generalised synchronisation exists between two dynamical systems X and Y when the state of the response system Y is a function of the state of the driving system X: $Y = F(X)$. If F is continuous, two close points on the attractor of X should correspond to two close points on the attractor of Y. An important feature of generalised synchronisation is that synchronised time series can look very dissimilar. This is in contradistinction to other measures (except MI), which require some similarity between time courses to detect interactions.

Since its proposal, several algorithms have been developed to detect generalised synchrony in experimental time series (Arnhold et al., 1999; Quian Quiroga et al., 2002; Rulkov et al., 1995; Schiff et al., 1996). They all rely upon some time-delay embedding (Takens, 1981). This method reconstructs the state space using m-dimensional vectors whose components are con-

secutive values of the signals $\overrightarrow{X}_n = [x_n, x_{n+\tau}, \ldots, x_{n+(m-1)\tau}]$, $\overrightarrow{Y}_n = [y_n, y_{n+\tau}, \ldots, y_{n+(m-1)\tau}]$, $n = 1, \ldots, N'$, where $N' = N - (m-1)\tau$, m is the embedding dimension and τ is the delay time. A proper reconstruction of the state space depends upon the choice of m and τ. The embedding dimension m must be large enough to encompass the attractor but as small as possible to limit computational load. In the following, we used a geometrical method to determine m. This procedure is based on minimising the number of false nearest neighbours (Kennel et al., 1992). The delay time parameter τ was chosen, as is convention, to be the first zero of the autocorrelation function of the signals. Note that a geometric approach can also be adopted to determine the optimal τ, which is generally not independent of the optimal m (Rosenstein et al., 1994). A crucial aspect of all measures based upon temporal embedding is the exclusion of vectors pairs that are proximate simply because they are close in time. Consequently, pairs $[\overrightarrow{X}_{n_1}, \overrightarrow{X}_{n_2}]$ are excluded when $|n_1 - n_2|$ is lower than some threshold, called the Theiler correction (Theiler, 1986). We used a Theiler correction equal to τ.

In many systems, the function F is generally unknown. However, its form is not essential for detecting interdependencies since the existence of F induces a particular relationship among the neighbourhood structure of states on the attractors of coupled systems. This structure can be measured in terms of (i) closeness between $\overrightarrow{X}_n$ and its corresponding actual and mutual neighbours using the geometric definition of distance (Arnhold et al., 1999; Quian Quiroga et al., 2002), (ii) mutual prediction (for instance, estimation of $\overrightarrow{Y}_{n+\delta}$ knowing $\overrightarrow{X}_n$ and its neighbours) (Schiff et al., 1996) and (iii) synchronisation likelihood (Stam and van Dijk, 2002), which is closely related to the concept of generalised mutual information. We present and use only the first of these measures (results obtained using the others were qualitatively very similar) and, for simplicity, refer to it as the generalised synchronisation measure or generalised synchrony. However, it should be noted that generalised synchronisation is a concept rather than a measure.

Let $n_{\overrightarrow{X}_n}^j$ and $n_{\overrightarrow{Y}_n}^j$, $j = 1, \ldots, k$, denote the time indices of the k nearest neighbours of $\overrightarrow{X}_n$ and $\overrightarrow{Y}_n$. By definition, $\{\overrightarrow{X}_{n_{\overrightarrow{X}_n}^j}\}_{j=1,\ldots,k}$ are the true neighbours of $\overrightarrow{X}_n$ and $\{\overrightarrow{Y}_{n_{\overrightarrow{X}_n}^j}\}_{j=1,\ldots,k}$ are the mutual neighbours of $\overrightarrow{Y}_n$ and vice versa for $n_{\overrightarrow{Y}_n}^j$. For each $\overrightarrow{X}_n$, the mean squared Euclidean distance to its k nearest neighbours is defined as

$$D_n^{(k)}(X) = \left\langle \left(\overrightarrow{X}_n - \overrightarrow{X}_{n_{\overrightarrow{X}_n}^j} \right)^2 \right\rangle_j \tag{8}$$

and the Y-conditioned mean squared Euclidean distance of $\overrightarrow{X}_n$ is defined by replacing the true nearest neighbours of $\overrightarrow{X}_n$ by the equal partners of the closest neighbours of $\overrightarrow{Y}_n$ (mutual neighbours of $\overrightarrow{X}_n$):

$$D_n^{(k)}(X \mid Y) = \left\langle \left(\overrightarrow{X}_n - \overrightarrow{X}_{n_{\overrightarrow{Y}_n}^j} \right)^2 \right\rangle_j. \tag{9}$$

If the systems X and Y exhibit generalised synchrony, then $n_{\overrightarrow{Y}_n}^j \approx n_{\overrightarrow{X}_n}^j$, and thus $D_n^{(k)}(X|Y) \approx D_n^{(k)}(X)$. Conversely, if the systems are independent then $D_n^{(k)}(X|Y) \approx D_n^{(N'-1)}(X)$ where $D_n^{(N'-1)}(X)$ is the mean squared Euclidean distance between point $\overrightarrow{X}_n$ and the remaining points $\overrightarrow{X}$. Several normalised measures have been defined (Arnhold et al., 1999; Quian Quiroga et al., 2002). We will use only one of these:

$$\Delta^{(k)}(X \mid Y) = \left\langle \frac{D_n^{(N'-1)}(X) - D_n^{(k)}(X \mid Y)}{D_n^{(N'-1)}(X)} \right\rangle_n \tag{10}$$

which is below but close to 1 when X and Y are synchronised and tends towards 0 when they are independent.

$\Delta^{(k)}(Y|X)$ is obtained in a similar fashion but is not identical to $\Delta^{(k)}(X|Y)$ for asymmetrical systems. This property can be used to estimate the driver and driven systems, although one should be careful interpreting $\Delta^{(k)}(Y|X) - \Delta^{(k)}(X|Y)$ (Pereda et al., 2001; Quian Quiroga et al., 2000).

Phase synchronisation measures

Phase synchronisation between two oscillators is a ubiquitous phenomenon, which appears when they are coupled in a broad range of structures, including MEG or EEG generators (Pikovsky et al., 2001). Consequently, time frequency analysis of phase synchronisation is popular in current research on cortical network identification in MEG or EEG (David et al., 2003b; Engel et al., 2001; Varela et al., 2001). Basically, phase synchronisation analysis proceeds into two steps: (i) estimation of the instantaneous phases and (ii) quantification of the phase locking.

Estimation of the instantaneous phases

There is an uncertain consensus about how to define the phase of a signal. In the MEG or EEG community, two equivalent methods are used: either the instantaneous phase of the MEG or EEG signal is taken to be the phase of its analytical signal obtained using the Hilbert transform, or it is identified by the phase of a complex wavelet transform using Gabor functions. It has been shown that both methods give similar results (Le Van Quyen et al., 2001; Quian Quiroga et al., 2002). Consequently, we will restrict our presentation to the Hilbert transform.

The analytic signal $\xi(t)$ of the univariate measure $x(t)$ is a complex function of continuous time t defined as (Rosenblum et al., 1996)

$$\xi(t) = x(t) + ix_h(t) = a_\xi(t)e^{i\phi_\xi(t)} \tag{11}$$

where the function $x_h(t)$ is the Hilbert transform of $x(t)$

$$x_h(t) = \frac{1}{\pi} \text{P.V.} \int_{-\infty}^{+\infty} \frac{x(t)}{t - \tau} d\tau. \tag{12}$$

P.V. indicates that the integral is taken in the sense of Cauchy principal value. $a_\xi(t)$ and $\phi_\xi(t)$ are the instantaneous amplitude and phase of the analytic signal $\xi(t)$ of $x(t)$. The instantaneous phase $\phi_x(t)$ of $x(t)$ is taken equal to $\phi_\xi(t)$. Identically, the phase $\phi_y(t)$ is estimated from $y(t)$.

The instantaneous phase, although defined uniquely for any kind of signal to which the Hilbert transform can be applied, is difficult to interpret physiologically for broadband signals. Moreover, it can be inefficient when looking for oscillations characterised by a weak energy in a particular narrow band. For these reasons, a standard procedure is to consider only narrow-band phase synchronisation by estimating an instantaneous phase for successive frequency bands, which are defined by band-pass filtering the time series (Le Van Quyen et al., 2001).

Phase-locking quantification

For independent time series $x(t)$ and $y(t)$, the distribution of the relative phase $\phi_{xy}(t) = \phi_x(t) - \phi_y(t)$ is uniform within a given time window whose width defines the time resolution of the analysis

(usually a few hundred milliseconds). The detection of phase locking involves quantifying the divergence from uniformity of the relative phase distribution. Several measures have been proposed for this purpose (Lachaux et al., 1999; Tass et al., 1998). We will consider the one used in (Lachaux et al., 1999):

$$\rho = \left| \left\langle e^{i\phi_{xy}(t)} \right\rangle_t \right| \tag{13}$$

where ρ is the mean phase coherence of an angular distribution (Mormann et al., 2000). By construction, it is bounded by 0 (no synchronisation) and 1 (perfect synchronisation).

Evaluation of dependency measures with a neural mass model

In this section, we evaluate the sensitivity of the measures described in the previous section using a neural mass model of coupled cortical regions (David and Friston, in press). This model is based upon several simplifying assumptions, partly limiting its validity, but it still serves as a useful vehicle to understand some general features of macroscopic brain signals. The major assumption of that model is the so-called mean field approximation, which considers that variables of the model represent the average behaviour of quantities of interest, over the neuronal populations. In other words, there is no explicit spatial dimension since neurons belonging to a same neuronal assembly all express themselves through the population dynamics (of the mean). This entails some approximations to the underlying dynamics that can be evaluated using more sophisticated approaches based upon population densities (Haskell et al., 2001). Thus, neural mass models deal with massive interactions at a macroscopic scale and are generally unable to model microscopic spatiotemporal patterns at the neuronal level.

Fig. 1 provides a schematic description of the model when two areas are coupled. This is the case considered below. The input of each area acts upon dendrites of pyramidal cells, and not of excitatory spiny stellate cells as falsely indicated in (David and Friston, in press). The MEG or EEG signal is computed the level of apical dendrites. Each area i ($i = 1,2$) is characterised by a parameter w_i, bounded between 0 and 1, which scales the contribution of populations with slow and fast time constants to the area's dynam-
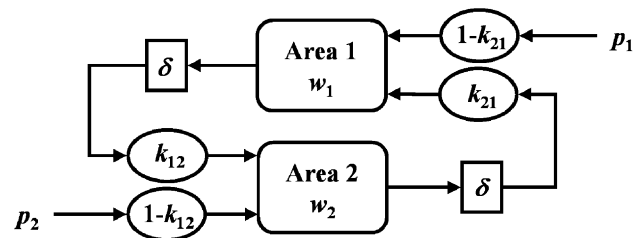
Fig. 1. Schematic of the neural mass model (David and Friston, in press). The intrinsic dynamics of each area i are controlled by a parameter w_i that regulates the relative contributions of subpopulations with fast and slow kinetics. Areas are coupled with a propagation delay δ and a coupling coefficient k_i ($0 \le k_i \le 1$), which controls the contribution of one area to the other, relative to extrinsic inputs. These inputs p_i are stochastic innovations and represent the influence of the rest of the brain. Simulations were performed with the following values: $w_1 = w_2 = 0.8$, $\delta = 10$ ms, $<p_1> = <p_2> = 220$, std(p_1) = std(p_2) = 22. Detailed equations of this model are provided in Appendix A.

ics. The input of each area i is a mixture of the output of the other area j (delayed by a propagation time δ) and a stochastic innovation p_i (Gaussian noise), which simulates afferents from the rest of the brain. The contribution of inputs from the other area is specified by the coupling coefficients k_{ij} bounded between 0 (no coupling) and 1 (stochastic inputs ignored). A detailed description of MEG or EEG signals generated by this model can be found in (David and Friston, in press). For completeness, the equations used for the simulations are provided in the Appendix A.

For simplicity, we consider a symmetric configuration ($k = k_{12} = k_{21}$, $w = w_1 = w_2$). The parameters w and δ were set to 0.8 and 10 ms, respectively. These parameters generate signals showing a realistic ratio in the alpha and beta bands for a broad range of coupling values k (Fig. 2). The coupling sensitivity of dependency measures was evaluated using simulated MEG or EEG time series obtained for different values of the coupling coefficient k. We varied k between 0.025 and 1 using a step size of 0.025. For each value of k, 20 realisations of time series were obtained, each of 1-s duration. When coupled, the signals generated by that model tend to oscillate in phase or antiphase as shown in David and Friston (in press). Accordingly, the cross-correlation was evaluated with a time lag $\tau = 0$. The number of bins I used to compute the mutual information MI was set to the number just below $\ln(N)/\ln(2)$. Because of the symmetric configuration, the generalised synchronisation measure Δ was taken arbitrarily to be $[\Delta(X|Y) + \Delta(Y|X)]/2$. The embedding dimension m used to compute Δ was estimated to be 3 and the size of the neighbourhood set to $2m$, which is large enough to avoid spurious effects of changes in signal complexity in the quantification of interactions (Pereda et al., 2001).

We assessed overall sensitivity to coupling in terms of the changes in each measure induced by changes in k. To establish a statistical bound on the sensitivity, the null distribution of each measure was determined using surrogate data with no coupling. To assess the sensitivity to the nonlinear component of coupling, we computed each measure before and after destroying high-order dependencies using phase randomisation.

Coupling sensitivity

The model parameters were chosen to generate broadband signals that generally expressed two well-defined frequency bands as shown in Fig. 2. It is possible to analyse these signals as such (broadband analysis) or using a bank of narrow band-pass filters. This is often done when studying oscillations (narrow-band analysis). Below, we report the coupling sensitivity of the dependency measures (cross-correlation, mutual information, generalised synchronisation and phase synchronisation) using both approaches. The characteristics of interaction measures were evaluated by comparing their distributions obtained using coupled time series ($k \neq 0$) and 100 surrogate time series generated with no coupling ($k = 0$).

Broadband analysis

Fig. 3a shows the dependence of interaction measures on coupling strength. The black solid curve is the average, over realisations, of the measures $\mu(k)$ as a function of coupling strength k. The standard deviation $\sigma(k)$, normalised by the mean of the estimators, is plotted in grey. This is the coefficient of variation C.V. The C.V. reflects the intrinsic variability of the measures in relation to their size. A small C.V. suggests that one may be able to correlate the connectivity indices with other measures of brain state. An example of this is provided in the last section. A high C.V. compromises the usefulness of the measure when detecting changes in coupling.
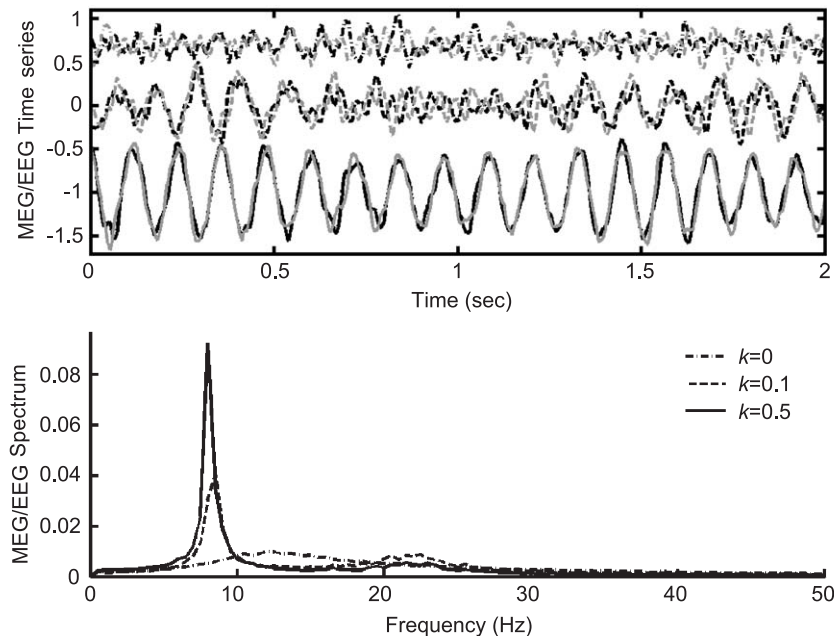
Fig. 2. Some typical simulated MEG or EEG time-series are shown in the top panel for different values of the coupling strength k ($k = 0$: dash dot line; $k = 0.1$: dashed line; $k = 0.5$: solid line; model parameters: $w = 0.8$, $\delta = 10$ ms). The DC offset has been modified for a better display. The sampling frequency is 1 ms. Below is the average amplitude spectrum of 20 simulated time series without DC offset, obtained with the same parameters. The neuronal time constants and the parameters w and δ were chosen to generate power in the alpha (8–12 Hz) and beta (15–30 Hz) bands to emulate the typical MEG or EEG spectrum. Strikingly, the shape of the spectra depends critically on the coupling parameter k.

a

b

$$1 - \alpha = p(x < u \mid k = 0) \qquad \beta = p(x \geq u \mid k \neq 0)$$

specificity   *sensitivity*
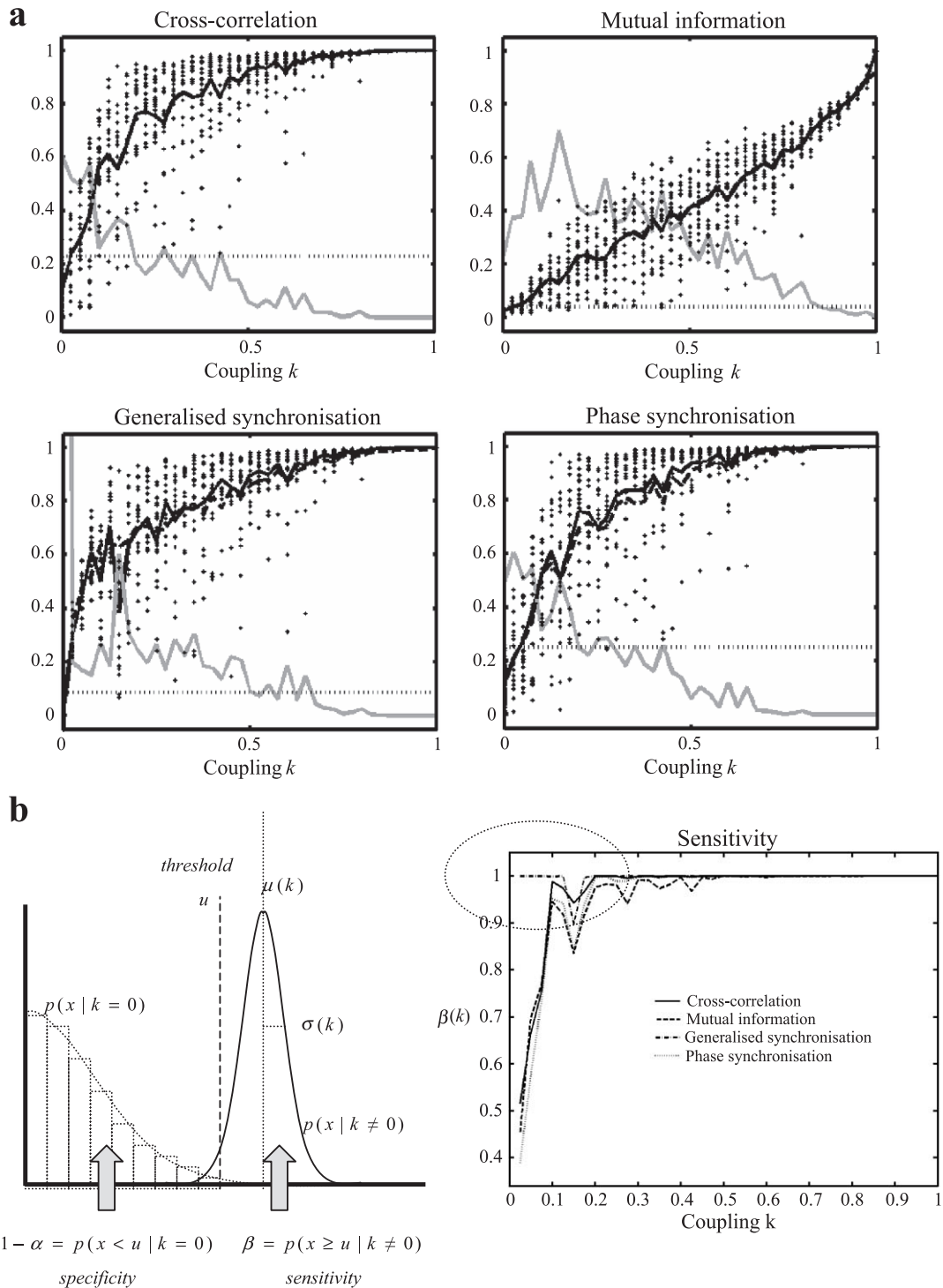
Fig. 3. (a) Dependency measures applied to broadband signals as an increasing function of the coupling, as shown by solid lines (average value) over 20 realisations (dots). Cross-correlation, mutual information and phase synchronisation are less sensitive to weak couplings than generalised synchronisation. The dotted line represents the maximum value obtained from 100 realisations of uncoupled time series ($k = 0$) and corresponds to a nominal specificity $\alpha = 0.01$. The dotted lines are the same measures but obtained with surrogate data that retained only the linear properties of original time series. cross-correlation and mutual information show little sensitivity to nonlinear properties of data (the solid and dotted lines are almost coincident). As expected, nonlinearity is detected by generalised synchronisation and by phase synchronisation but only for strong coupling. (b) Left: schematic illustrating how we computed sensitivity. This is based on simple signal detection theory using threshold to control specificity. This threshold u is based on the empirically determined null distribution (using surrogate data). The area under the density $p(x \mid k \neq 0)$ between u and infinity corresponds to the probability of detecting coupling when it exists. This threshold also ensures that the false positive rate (or specificity) is maintained at 0.01. Right: sensitivity as a function of coupling for each of the four measures. It is self-evident that generalised synchrony supervenes at low connection strengths (see encircled region).

The dotted line indicates the maximum value obtained using surrogate data. This is the nonparametric threshold for a false positive rate of $\alpha = 0.01$ for a single measure and will be called u below. The reason the specificity $\alpha = 0.01$ is that we used 100 realisations of the surrogate data to form an empirical null distribution. The power or sensitivity β at this specificity $(1 - \alpha)$ is simply the probability of any measure exceeding u under the alternate hypothesis that $k \neq 0$. We can approximate this for each level of k by assuming a Gaussian form for the distribution of measures and using their sample mean and variance. Fig. 3b provides a schematic illustration of the sensitivity analysis (left panel). The right panel shows sensitivity $\beta(k)$ as a function of coupling for each of the measures.

At a first glance, we observe that every measure was sensitive to changes in neuronal coupling. However, some differences are seen. Apart from mutual information, all the measures exhibit a similar profile, on average (quasi-linear dependence upon coupling before saturating at large coupling values), and approximately the same coefficient of variation. The mutual information shows a quasi-linear dependence upon coupling but is a less reliable metric as indicated by its larger C.V. The cross-correlation and the phase synchronisation show very similar behaviours. In terms of weak coupling values are concerned $(0 < k = 0.125)$, generalised synchronisation is the best measure for detection (i.e., making an

inference that $k \neq 0$). This is clearly evident from the right panel of Fig. 3b. On the other hand, mutual information may be a better characterisation in the context of strong coupling because it has a relatively low coefficient of variation and retains sensitivity to changes in k, that is, the slope $\partial \mu (k) / \partial k$ is much greater relative to the other measures.

Another important property of the interdependency measures is their time resolution. A characteristic feature of functional connectivity in the brain is its tendency to fluctuate rapidly; synchronous cells assemblies are formed and dissolved at subsecond time scales (Friston, 2000; Varela et al., 2001). To evaluate the time resolution of the coupling measures, we varied the length of the time window applied to signals used in Fig. 3 from 0.2 to 2 s with a step size of 200 ms. We used $k = 0.1$ (Fig. 2) to produce signals that resemble real MEG data. We compared the coupling values to those obtained with surrogates $(k = 0)$ by computing z-scores (i.e., the mean divided by the standard deviation under the null hypothesis). Fig. 4 shows that the statistical power of coupling detection is an increasing monotonic function of window length. The slopes for mutual information and generalised synchronisation are larger. This suggests that these measures are relatively more efficient with longer time windows that are used to characterise stable regimes. Moreover, the variance of the generalised synchronisation measure is smaller, indicating a more sensitive
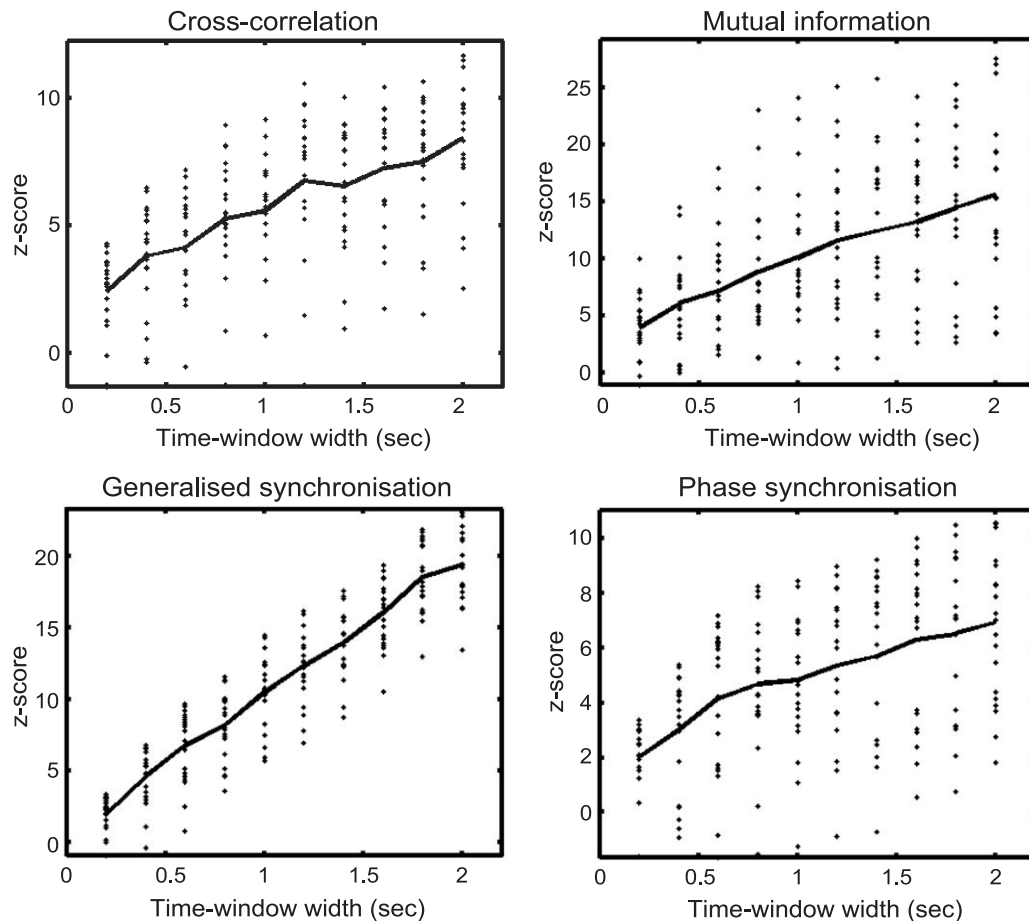
Fig. 4. Coupling detection power as a function of the length of the time series. To evaluate the time resolution of coupling measures, we varied the length of the time window applied to signals (with $k = 0.1$), from 0.2 to 2 s, with a step size of 200 ms. We compare the coupling values to those obtained with surrogates $(k = 0)$ by computing z-scores. The slopes for mutual information and generalised synchronisation are larger reflecting a relatively greater efficiency for long-time windows relative to short one. Moreover, the variance of the generalised synchronisation measure is smaller indicating a more reliable estimator.

detection in the context of stationary coupling. In a subsequent paper, we will revisit this issue using evoked neuronal transients that are, by definition, nonstationary.

In summary, the generalised synchronisation measure appears to be the most sensitive for detecting interactions between broadband simulated MEG or EEG signals under continuous recording conditions. Conversely, mutual information retains the greatest sensitivity to changes in coupling at higher levels.

Narrow-band analysis

To supplement the broadband analysis, we performed narrow-band analyses from 2 to 50 Hz, with a step size of 2 Hz, encompassing the resonant frequencies of the model. For each frequency band, we used a band-pass filter constructed so that the central frequency/band width ratio was 5. The coupled ($k = 0.1$) and uncoupled ($k = 0$) time series were filtered and dependency measures were estimated as above. For each frequency band, the optimal embedding dimension m remained 3 but the delay time τ varied, changing with the first zero of the autocorrelation function. The results are summarised in Fig. 5 by plotting the z-scores of each statistic as a function of central frequency. The shape of the sensitivity profile of each statistic is very similar with peaks over the two frequency bands of prominent oscillations expressed by the neuronal populations in the model.

Strikingly, the mutual information z-scores were much higher than the other measures. This suggests that mutual information may be a more efficient (i.e., less variable) index of coupling in the context of frequency-specific coupling.

In summary, all measures can be used to estimate interactions that are localised in frequency space, but mutual information has a much larger sensitivity. This allows one to identify the frequencies within which occur strong interactions. These frequencies depend on various network properties (neuronal time constants, propagation delays, coupling strength, neuronal architecture, etc.).

Sensitivity to nonlinearity

Nonlinearity is an important characteristic of MEG or EEG signals, especially when considered in the context of broadband processes. In our model, nonlinearity arises from the sigmoid relationship that maps the membrane potential to firing rate of neurons; this is equation $S(v)$ in the Appendix A. However, it should be noted that the degree of nonlinear coupling in our model is fairly weak. Weak nonlinearities can be typical of normal EEG time series (Breakspear and Terry, 2002; Stam et al., 1999) in contradistinction to epileptic signals where nonlinearity supervenes (Lopes da Silva et al., 1989). An expedient way to detect
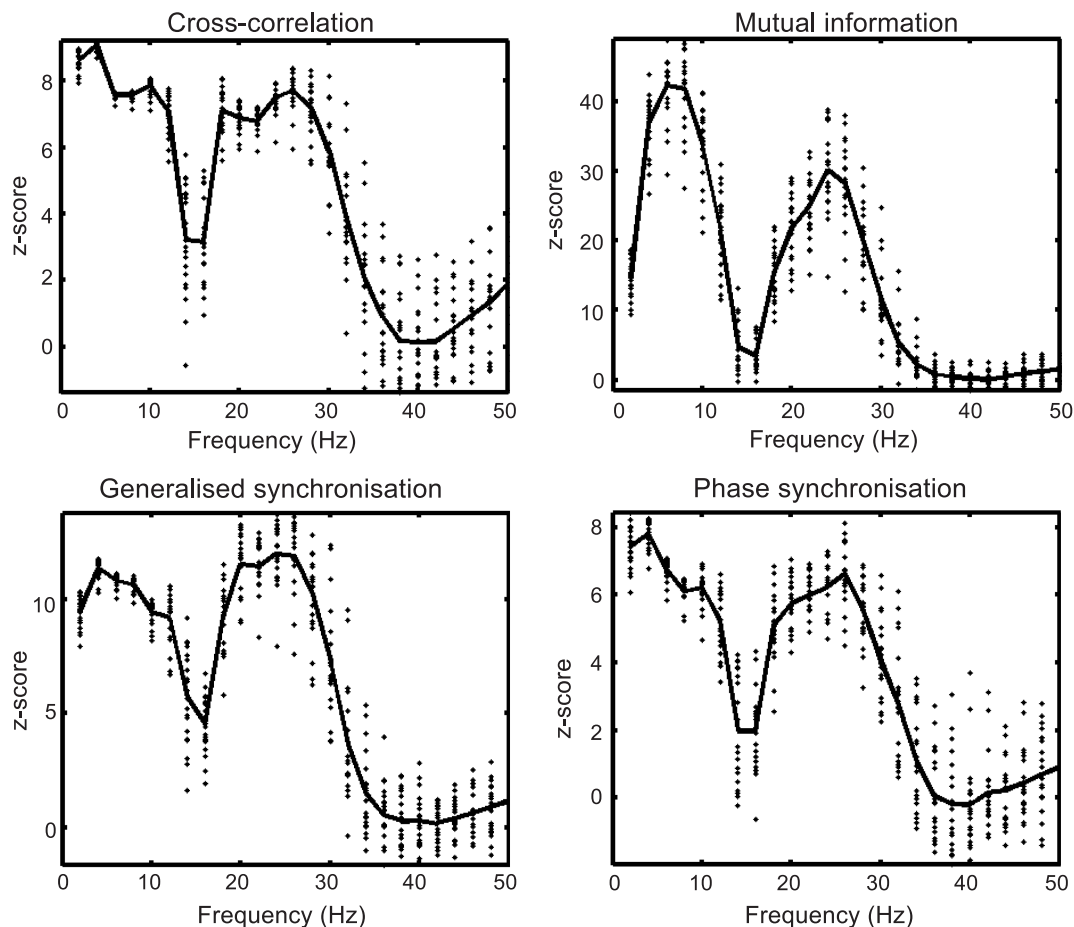
Fig. 5. Coupling sensitivity for narrow-band analysis. The original (coupled $k = 0.1$ and uncoupled $k = 0$) time series were filtered in different narrow frequency bands from 2 to 50 Hz, with a step size of 2 Hz, encompassing the resonant frequencies of the model (centre: width ratio = 5). The z-scores of each statistic are plotted as a function of central frequency. The sensitivity profile of each statistic is very similar, clearly highlighting the two frequency bands of interactions expressed by the neuronal populations in the model. The mutual information z-scores are much higher than the other measures.
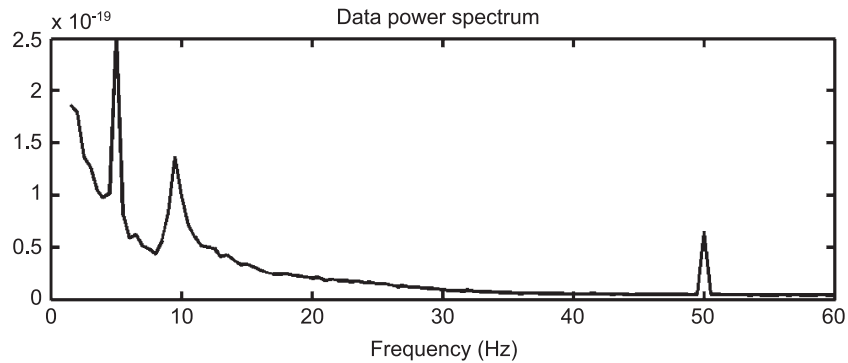
Fig. 6. Power spectrum of real MEG data. This spectrum was obtained after averaging over 151 channels and 50 successive segments of 2-s duration. The 5-Hz peak corresponds to the frequency tag introduced by visually presented expanding rings. It shows also a clear alpha band centred at 10 Hz, a flat beta band between 15 and 30 Hz (approximately) and a power supply artefact at 50 Hz.

nonlinearity is to apply the dependency measures to surrogate data that retain the linear properties of original data after destroying any nonlinear dependencies (Palus and Hoyer, 1998; Prichard and Theiler, 1994). These surrogates are realisations of a bivariate linear stochastic process that preserve the individual spectra of the two time series, as well as their cross spectrum. They are constructed by (i) computing the Fourier coefficients of original time series, (ii) adding an identical but random phase $\varphi(\omega)$ to both coefficients of the same frequency bin ω [where $\varphi(\omega) = -\varphi(-\omega)$] and (iii) performing the inverse Fourier transform.

We applied this surrogate method to the simulated broadband signals and repeated the test for each of the four measures as a function of coupling strength. The dashed line in Fig. 3a represents average measures over 20 surrogates. The difference between the statistics with (solid) and without (dashed) nonlinear coupling reflects the relative sensitivity to nonlinear interdependencies. By definition, the cross-correlation is insensitive to nonlinear inter-actions and the dashed and solid lines are indistinguishable. The mutual information does not show any significant nonlinear component. However, generalised and phase synchronisation measures are sensitive to nonlinear interactions, which account for a small component of their value.

In summary, these results suggest that although all measures are sensitive to neuronal coupling, they do not behave identically. Overall, generalised synchrony appears to be the most appropriate measure because of its relatively high sensitivity in the context of weak coupling and sensitivity to nonlinear coupling. However, it entails very high computational demands in comparison to the other methods and may not be robust to nonstationariness. It follows that the choice of measure is a crucial determinant of functional connectivity architecture that is operationally defined by

its measurement, particularly in broadband analyses. Below we analyse an MEG data set to illustrate this point and show how the cortical networks identified can change substantially with the measure of functional connectivity employed.

Application to binocular rivalry MEG data

Binocular rivalry occurs when nonfusible stimuli are presented to each eye simultaneously. The outcome is not a superposition of both stimuli but a spontaneously alternating perception of each monocular stimulus. Dominance periods, for each percept, last about one or 2 s before perceptual transition (for a review, see Blake and Logothetis, 2002). Studying data obtained during binocular rivalry is well suited to our purpose because neural signals are produced under conditions that are close to our simulations: (i) binocular rivalry must arise in the context of substantial changes in neural interactions, as the stimulus always remains constant, and (ii) the perceptual dynamics evolves at a slow time scale, allowing the use of nonlinear methods that rest on local stationariness for efficient estimation.

Experimental design

This experiment was performed at the MEG Centre, La Salpê-trière Hospital, Paris, France, using a whole-head 151 sensors MEG system (CTF Inc., Vancouver, Canada). The stimuli composed an emotionally neutral face and a set of checkerboard rings expanding at 5 Hz. Stimuli were presented dichoptically using polarised projection. The primary motivation for using expanding rings was to tag MEG responses at the stimulus frequency (Srinivasan et al.,
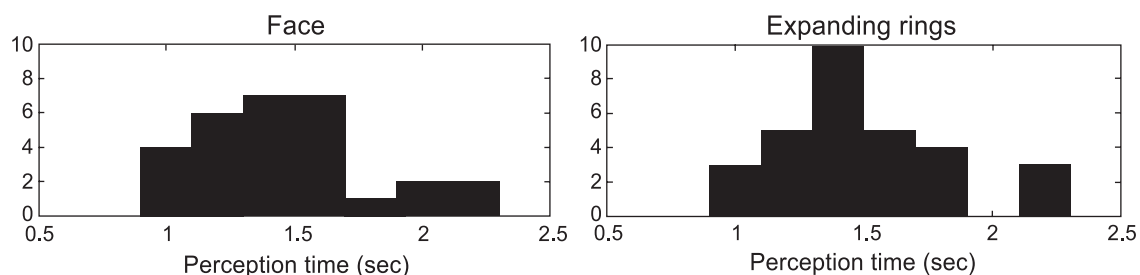
Fig. 7. Frequency histograms of dominance periods (29 for face, 30 for rings). On average, the dominance period for rings and faces are roughly the same (1.53 vs. 1.46 s).
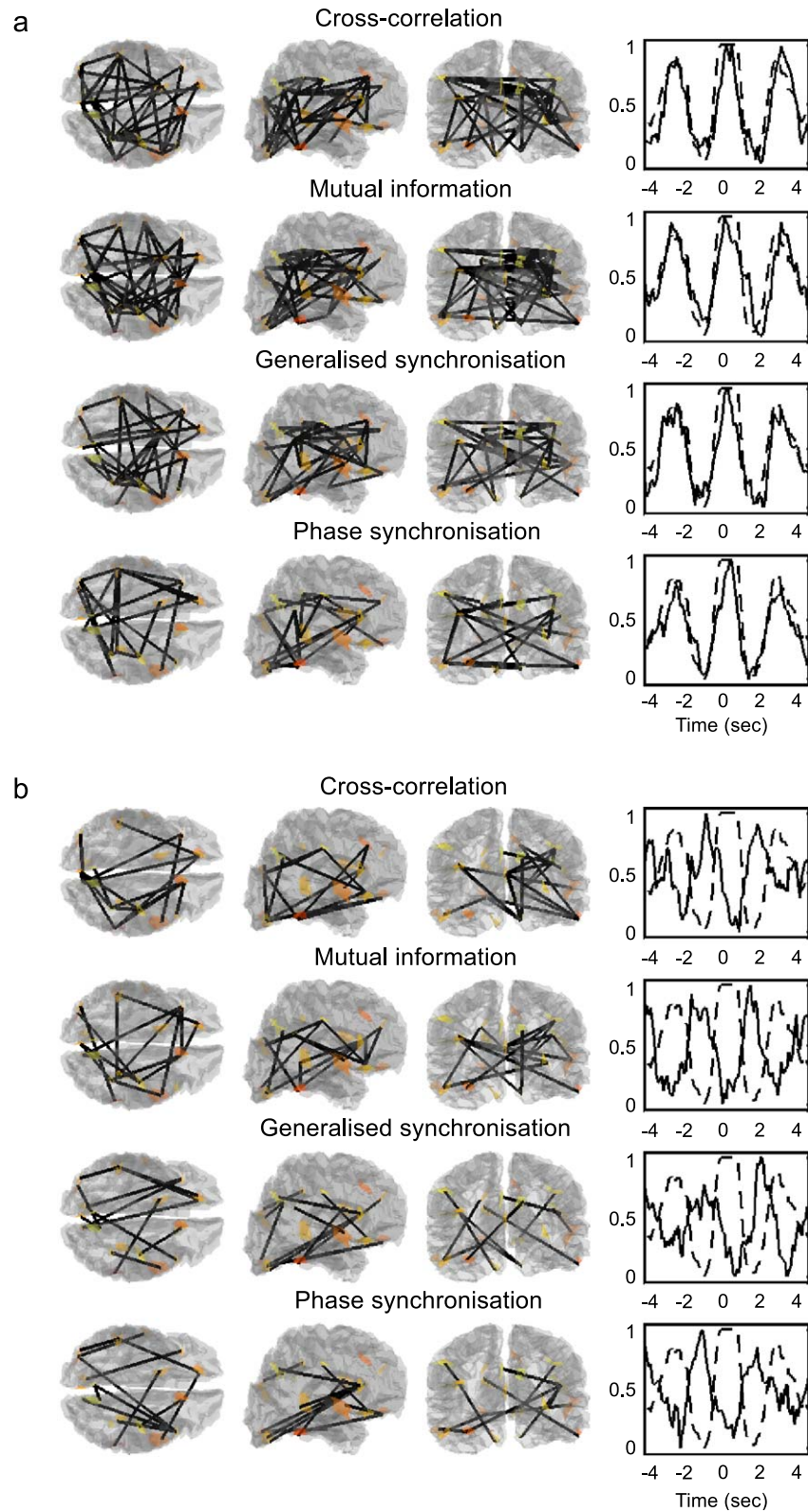
Fig. 8. Cortical networks related to the face perception (a) and to ring perception (b), estimated using several dependency measures. The cortical connections were estimated by applying a threshold ($P < 0.005$ where the null distribution was determined using surrogate data) to the correlation between the dependency measures and the face perception function (dashed lines) averaged over a 9-s time window. The solid lines on the right are the coupling time series averaged over the selected cortical connections. Networks correlated with face perception are much more extensive than those correlated to ring perception. The time series also show a stronger correlation between cortical interactions and perceptual state for faces. The networks based on cross-correlation and mutual information tend to be denser.

1999). It has been shown that the conscious percept of 5 Hz expanding rings modulates the MEG spectrum at the same frequency (Fig. 6). This entrainment is enabled by the retinotopic organisation of visual areas (David et al., 2003a). This tagging is an interesting dynamical phenomenon during binocular rivalry (Cosmelli et al., in preparation), but it is an artefact from our perspective. In addition to the 5-Hz component, the data power spectrum in Fig. 6 shows a clear alpha band centred at 10 Hz, a rather flat beta band and a power supply artefact at 50 Hz. We therefore focused, arbitrarily, on signals in the beta band (15–30 Hz).

The MEG data were acquired for 100 s at a sampling frequency of 1250 Hz. The subject indicated perceptual state (rings or face) with a button press. Twenty-nine periods of face dominance were reported, while 30 were attributed to the rings. The frequency histograms of dominance periods are shown in Fig. 7. On average, the dominance periods for rings and faces were about the same (1.53 vs. 1.46 s). The subject's report enabled us to construct a face perception time series (equal to 1 for face dominance and 0 for ring dominance).

Source localisation and dynamics estimation

The MEG data were band-pass filtered in the beta band (between 15 and 30 Hz), and source localisation procedures were applied to estimate cortical dynamics. Sparse focal, cortically distributed solutions were reconstructed using inverse methods described elsewhere (David and Garnero, 2002; David et al., 2002, 2003a). The resulting 22 sources are shown in Fig. 8. Each source corresponds to a single time series, obtained using the classical minimum norm estimator (Dale and Sereno, 1993; David and Garnero, 2002). Bilateral activations were found in lingual gyrus, precuneus, cingulate gyrus, orbital cortex (posterior and medial orbital gyrus), inferior frontal gyrus or frontal operculum, posterior inferior temporal gyrus and intraparietal sulcus. Exclusive right hemisphere activation was found in the anterior portion of the superior temporal gyrus and the central sulcus. In the left hemisphere, responses were detected in the cuneus, middle occipital gyrus, middle temporal gyrus and angular gyrus.

It is important to note that the dynamics of localised sources depend upon the source configuration since the lead fields are not orthogonal. This means that in principle, if one source is not detected by the localisation procedure, then its contribution to the surface data may be reallocated in part to other sources. This is a tricky issue that cannot be entirely avoided due to the ill-posed nature of the MEG or EEG inverse problem (Baillet et al., 2001).

Functional connectivity analysis

Neuronal interactions were estimated among reconstructed sources using the measures considered above. A sliding time window (1 s width, 100 ms between successive windows) was used to reconstruct a time-dependent measure of functional connectivity. To ensure that the results were comparable to the simulations, the asymmetry of generalised synchronisation measure Δ was discounted by defining $\Delta = [\Delta(X|Y) + \Delta(Y|X)]/2$. Moreover, the same embedding dimension and neighbourhood size were used.

We were particularly interested in whether time-dependent changes in coupling were correlated to conscious perception. To assess this, we computed the correlation between the dependency measures and the subject's perceptual state. The average perception function, computed over a 9-s time window, is shown as the dashed lines on the right side of Fig. 8 (large values correspond to face perception).

For each perceptual state and dependency measure, the connections that were significantly correlated with perception were used to define the perceptual network (Fig. 8). This was achieved using the cross-correlation between dependency measures and perceptual state. The threshold was determined nonparametrically using surrogates. Two hundred surrogate data sets were constructed by averaging time series using the same number of time windows but randomly in time. Each surrogate was correlated to the average perception function and the threshold for each source pair was taken to be the maximum of this quantity over realisations (i.e., $P < 0.005$).

Fig. 8 presents the networks identified in this fashion, for each dependency measure. The networks are shown separately for positive correlations with face perception (Fig. 8a) and negative correlations (i.e., positive correlations with rings; Fig. 8b). As can be seen in the left panels of Fig. 8a, all four measurements show a good correlation with face perception. Likewise, the networks show important similarities in their overall distribution. All the networks share a common pattern of interaction among occipital, inferior parietal, posterior inferior temporal, middle temporal and frontal regions, in particular, inferior lateral frontal cortices and medial frontal regions including the cingulate cortex. However, the density of perception-related changes in coupling varies with the different measures. While cross-correlation and mutual information reveal a dense network of interacting regions, generalised synchronisation and, in particular, phase synchronisation show a more diffuse set of connections. In the specific case of phase synchronisation, the right inferior frontal region connections are particularly sparse. On the other hand, when the subject perceives the rings, the identified networks (Fig. 8b), although present, are consistently smaller. cross-correlation and mutual information still reveal more percept-dependent coupling relative to synchronisation measures.

It is obviously impossible to conclude which functional connectivity measure is the best with a single subject analysis. However, the results shown above demonstrate strong correlations between perceptual states and coupling as inferred using distant MEG signals. They also confirm that dependency measures can be a critical factor when characterising functional connectivity in MEG or EEG.

Discussion

The purpose of this study was to (i) assess the relative sensitivity of commonly used measures of functional connectivity and (ii) to show that there is no unique measure of neural interactions using MEG or EEG signals. We used a neural mass model to show that several measures detect functional connections but with different sensitivity profiles. In the context of relatively weak coupling, statistics based on generalised synchrony appear to be the most sensitive. We have shown, with real MEG data, that the choice of dependency measure can be important for the identification of functional networks.

The neural mass model we used was developed to obtain a qualitative characterisation of oscillatory dynamics in MEG or EEG signals and how these change with the coupling among areas

(David and Friston, in press). Although its basic architecture is neurophysiologically plausible, it does not accommodate many details of neuronal interactions. However, it generates mildly nonlinear signals that are very similar to empirical signals (Breakspear and Terry, 2002; Stam et al., 1999). In this paper, we used the model to show that linear measures are sensitive to coupling between MEG and EEG signals but insensitive to nonlinear components. In contradistinction, generalised synchronisation and phase synchronisation were sensitive to both linear and nonlinear coupling. Furthermore, generalised synchrony was substantially more sensitive than any other measure when detecting very weak coupling.

Our results indicate that measures based on generalised synchronisation may be preferred when studying broadband signals because they are sensitive to dynamic coupling and nonlinear interactions expressed over many frequencies. However, they entail some drawbacks. First, they are time consuming. Second, they depend upon some parameters (time delay, embedding dimension and neighbourhood size) that are not always easily optimised. More importantly, if we consider two time series with a coupling that is kept exactly the same, but some other property (for instance the dimensionality) of one changes, almost all measures will be fooled and suggest a change in the coupling strength has occurred (Pereda et al., 2001). In view of the nonstationary nature of brain dynamics, this is not a trivial or hypothetical problem. For these reasons, linear measures are still very useful because they afford a rapid and straightforward characterisation of functional connectivity.

In general, reentrant loops that predominate widely in the brain generate resonant frequencies that reflect network properties (synaptic time constants, propagation delay, coupling strength, neuronal architecture, etc.). This has led to the search for frequency-specific interactions in MEG or EEG signals using measures such as coherence (Bressler, 1995; Gross et al., 2001), power (Tallon-Baudry and Bertrand, 1999) and phase synchronisation (Rodriguez et al., 1999). A growing number of studies have disclosed robust frequency-specific patterns, which are still not clearly understood. In particular, some relationship might exist between the oscillation frequency and the size of the networks involved (von Stein and Sarnthein, 2000). To analyse frequency-specific interactions, we used our model to generate complex signals whose interactions were confined largely to two distinct frequency bands. The dependency measures showed a corresponding and consistent frequency dependence, particularly with mutual information. This suggests that narrow-band analyses might supplement the characterisation of the underlying neuronal processes.

We have analysed MEG data using several characterisations of functional connectivity. We were particularly interested in neuronal interactions in the beta band (15–30 Hz) related to face and ring perception during binocular rivalry. We used source localisation algorithms to estimate cortical activity and searched for interactions among reconstructed cortical sources throughout the brain. Our results suggest that interdependencies among occipital, inferior parietal, posterior inferior and middle temporal, medial and inferolateral frontal cortices correlate strongly with the dominance of the face percept. The results presented here were obtained from one subject and little generalisation is possible. However, the patterns of interaction disclosed involve cortical regions that have been implicated in visual perception at several levels. Basic low-level processing of visual stimuli is associated with primary visual cortex activation (Tong, 2003). The perception of faces has been shown to implicate the inferior temporal cortex, in particular the fusiform gyrus (Halgren et al., 2000). In conjunction with parietal cortices, the cingulate cortex is believed to play a major role in the direction of attention to extrapersonal stimuli and conscious perception (Dehaene and Naccache, 2001; Mesulam, 1999). We have studied networks of interdependent cortical regions using a multistable perception paradigm in which the perception of a face is a spontaneous, endogenously driven phenomenon. Such processes necessitate the active coordination of recognition and other mechanisms required for perceptual categorisation, such as those mediated by striate and extrastriate visual cortex. In addition, high-level top-down influences, implicated in the selection and maintenance of percepts (Blake and Logothetis, 2002), are likely to be invoked. The distributed network obtained in this subject speaks to a dynamic coordination among such low- and high-level areas during the conscious perception of a face. Furthermore, it agrees with studies that show parietofrontal regions express correlates of perceptual transitions in a similar paradigm (Lumer and Rees, 1999; Lumer et al., 1998).

Our results also suggest that the exploration of the beta band (15–30 Hz) could be of interest for the study of long-range interactions in the human brain during perception. However, it is important to note that the functional networks identified exhibited differences from one measure to another. In particular, cross-correlation and mutual information revealed very dense networks, while generalised and phase synchronisation disclosed sparser patterns, probably because these measures may be intrinsically more variable (phase synchronisation) or stochastic aspects of the time series may confound the generalised synchrony measure.

In this paper, we have used a neural mass model to evaluate the relative sensitivities of various measures of coupling among neuronal systems. Clearly, the extent to which our conclusions can be generalised to the analysis of real data rests upon the biological validity of the model employed. It will be noted that although there are many similarities between the simulated and real data, there are also differences (e.g., in terms of the spectral density profile). Establishing the validity of models, such as the one we have used, is an important but difficult issue. One obvious approach is to use the model parameters that enable simulated data to emulate key features observed in empirical data. However, even this can be challenging at times. For example, as seen in Fig. 2, changes in key parameters such as the coupling strength can have quite a substantial impact on characterisations, such as the spectral density. In this paper, the model has been used to provide a proof of principle that different metrics are sensitive to different aspects of coupling. We appeal to the neuronal plausibility of the model's architecture in motivating this demonstration. However, the analysis of the empirical MEG data should not be interpreted quantitatively in relation to the simulations. This is because our model was not constrained to reproduce the exact characteristics of the particular MEG data set analysed. The main point that we wanted to make was that in both simulations and analyses of real data, different conclusions are obtained when using different measures of coupling.

The largest difference between results obtained on simulated and real signals is the performance of the measure based on the concept of generalised synchronisation. This is not new as the application of some of these methods in simple experimental

models has not been straightforward. The main reason is that MEG or EEG signals cannot be supposed as purely deterministic processes and their stochastic component can strongly affect the results. Another possibility is that such measures can be more sensitive to experimental artefacts that may be important in non-averaged MEG or EEG signals (especially muscular artefacts in the beta band). Nevertheless, nonsymmetrical nonlinear measures are very important, particularly for the estimation of causality or direction of information transfer (Chavez et al., 2003; Quian Quiroga et al., 2000; Wendling et al., 2001).

Conclusion

We have shown that neural mass models can be useful tool to evaluate measures of neural coupling in MEG or EEG signals. We have evaluated several commonly used dependency measures and demonstrated that their sensitivity depends upon (i) the frequency specificity of coupling (broad vs. narrow band) and (ii) the nature of the functional connectivity (linear vs. nonlinear). The differences in functional connectivity analyses, using real data, confirm differences in sensitivity profiles and speak to a substantial degree of coupling induced by face perception. The results of this study suggest that estimation of neuronal coupling is far from trivial and that one should be careful when studying functional connectivity using electrophysiological signals. As cautioned by others (Netoff and Schiff, 2002; Quian Quiroga et al., 2002), one should not make too many prior assumptions about the type of interactions. Applying a battery of tests that are sensitive to different aspects of synchronisation seems to be a more appropriate and balanced approach.

Acknowledgments

Appendix A

The model summarised in Fig. 1 composes the following stochastic differential equations. A more intuitive explanation of these equations will be found in David and Friston (in press).

$$\dot{y}_0 = y_3$$

$$\dot{y}_1 = y_4$$

$$\dot{y}_2 = y_5$$

$$\tau_e^1 \dot{y}_3 = H_e^1 S(w y_1 + (1-w)y_{10} - w y_2 - (1-w)y_6) - 2y_3 - y_0/\tau_e^1$$

$$\tau_e^1 \dot{y}_4 = H_e^1 (k_{21}^*(S(w(y_{13}(t-\delta) - y_{14}(t-\delta)) + (1-w)(y_{22}(t-\delta)$$
$$- y_{18}(t-\delta))) - a) + (1-k_{21})\tilde{p}_1 + p + C_2 S(C_1(w y_0$$
$$+ (1-w)y_8))) - 2y_4 - y_1/\tau_e^1$$

$$\tau_i^1 \dot{y}_5 = H_i^1 C_4 S(C_3(w y_0 + (1-w)y_8)) - 2y_5 - y_2/\tau_i^1$$

$$\dot{y}_6 = y_7$$

$$\tau_i^2 \dot{y}_7 = H_i^2 C_4 S(C_3(w y_0 + (1-w)y_8)) - 2y_7 - y_6/\tau_i^2$$

$$\dot{y}_8 = y_9$$

$$\tau_e^2 \dot{y}_9 = H_e^2 S(w y_1 + (1-w)y_{10} - w y_2 - (1-w)y_6) - 2y_9 - y_8/\tau_e^2$$

$$\dot{y}_{10} = y_{11}$$

$$\tau_e^2 \dot{y}_{11} = H_e^2 (k_{21}^*(S(w(y_{13}(t-\delta) - y_{14}(t-\delta)) + (1-w)(y_{22}(t-\delta)$$
$$- y_{18}(t-\delta))) - a) + (1-k_{21})\tilde{p}_1 + p + C_2 S(C_1(w y_0$$
$$+ (1-w)y_8))) - 2y_{11} - y_{10}/\tau_e^2$$

$$\dot{y}_{12} = y_{15}$$

$$\dot{y}_{13} = y_{16}$$

$$\dot{y}_{14} = y_{17}$$

$$\tau_e^1 \dot{y}_{15} = H_e^1 S(w y_{13} + (1-w)y_{22} - w y_{14} - (1-w)y_{18}) - 2y_{15}$$
$$- y_{12}/\tau_e^1$$

$$\tau_e^1 \dot{y}_{16} = H_e^1 (k_{12}^*(S(w(y_1(t-\delta) - y_2(t-\delta)) + (1-w)(y_{10}(t-\delta)$$
$$- y_6(t-\delta))) - a) + (1-k_{12})\tilde{p}_2 + p + C_2 S(C_1(w y_{12}$$
$$+ (1-w)y_{20}))) - 2y_{16} - y_{13}/\tau_e^1$$

$$\tau_i^1 \dot{y}_{17} = H_i^1 C_4 S(C_3(w y_{12} + (1-w)y_{20})) - 2y_{17} - y_{14}/\tau_i^1$$

$$\dot{y}_{18} = y_{19}$$

$$\tau_i^2 \dot{y}_{19} = H_i^2 C_4 S(C_3(w y_{12} + (1-w)y_{20})) - 2y_{19} - y_{18}/\tau_i^2$$

$$\dot{y}_{20} = y_{21}$$

$$\tau_e^2 \dot{y}_{21} = H_e^2 S(w y_{13} + (1-w)y_{22} - w y_{14} - (1-w)y_{18}) - 2y_{21}$$
$$- y_{20}/\tau_e^2$$

$$\dot{y}_{22} = y_{23}$$

$$\tau_e^2 \dot{y}_{23} = H_e^2 (k_{12}^*(S(w(y_1(t-\delta) - y_2(t-\delta)) + (1-w)(y_{10}(t-\delta)$$
$$- y_6(t-\delta))) - a) + (1-k_{12})\tilde{p}_2 + p + C_2 S(C_1(w y_{12}$$
$$+ (1-w)y_{20}))) - 2y_{23} - y_{22}/\tau_e^2 \quad \text{(A1)}$$

where

$$\text{Signal}_{\text{MEG}}^1 = w(y_1 - y_2) + (1-w)(y_{10} - y_6)$$

$$\text{Signal}_{\text{MEG}}^2 = w(y_{13} - y_{14}) + (1-w)(y_{22} - y_{18})$$

$$S(v) = \frac{e_0}{1 + \exp(r(v_0 - v))}$$

$$k_{12}^* = \frac{\sigma_p \sqrt{2k_{12} - k_{12}^2}}{\text{std}(S(w(y_1 - y_2) + (1-w)(y_{10} - y_6)))}$$

$$k_{21}^* = \frac{\sigma_p \sqrt{2k_{21} - k_{21}^2}}{\text{std}(S(w(y_{13} - y_{14}) + (1-w)(y_{22} - y_{18})))} \quad \text{(A2)}$$

with the following parameters: $a = 3.501$; $c = 135$; $c_1 = c_2 = 0.8c$; $c_3 = c_4 = 0.25c$; $H_e^1 = 3$; $H_e^2 = 7$; $H_i^1 = 20$; $H_i^2 = 150$; $\tau_e^1 = 0.0108$; $\tau_e^2 = 0.0046$; $\tau_i^1 = 0.022$; $\tau_i^2 = 0.0029$; $e_0 = 5$; $v_0 = 6$; $r = 0.56$; $\sigma_p = 22$; $p = 220$.

The input noise $\tilde{p}_{1,2}$ is Gaussian with standard deviation σ_p. These stochastic differential equations must be integrated numerically using appropriate procedures (Kloeden and Platen, 1999). In this paper, they were integrated using a standard second order Runge–Kutta algorithm that gave very similar results to those obtained with its stochastic version (Honeycutt, 1992). Note that the estimation of k_{12}^* and k_{21}^* is performed during the integration.

References

Abarbanel, H.D.I., Rabinovich, M.I., 2001. Neurodynamics: nonlinear dynamics and neurobiology. Curr. Opin. Neurobiol. 11, 423–430.

Abeles, M., 1991. Corticonics: Neural Circuits of the Cerebral Cortex. Cambridge Univ. Press, Cambridge.

Arnhold, J., Grassberger, P., Lehnertz, K., Elger, C.E., 1999. A robust method for detecting interdependences: application to intracranially recorded EEG. Physica, D 134, 419–430.

Baillet, S., Mosher, J.C., Leahy, R.M., 2001. Electromagnetic brain mapping. IEEE Signal Process. Mag., 14–30 (November).

Blake, R., Logothetis, N.K., 2002. Visual competition. Nat. Rev., Neurosci. 3, 13–21.

Boccaletti, S., Kurths, J., Osipov, G., Valladares, D.L., Zhou, C.S., 2002. The synchronization of chaotic systems. Phys. Rep. 366, 1–101.

Breakspear, M., Terry, J.R., 2002. Detection and description of non-linear interdependence in normal multichannel human EEG data. Clin. Neurophysiol. 113, 735–753.

Bressler, S., 1995. Large-scale cortical networks and cognition. Brain Res. Rev. 20, 288–304.

Buzuk, Th., Pawelzik, K., von Stamm, J., Pfister, G., 1994. Mutual information and global strange attractors in Taylor–Couette flow. Physica, D 72 (4), 343–350.

Chavez, M., Martinerie, J., Le Van Quyen, M., 2003. Statistical assessment of nonlinear causality: application to epileptic EEG signals. J. Neurosci. Methods 124, 113–128.

Clifford Carter, G., 1987. Coherence and time delay estimation. Proc. I.E.E.E. 75, 236–255.

Cosmelli, D., David, O., Lachaux, J.-P., Martinerie, J., Garnero, L., Renault, B., Varela, F., in preparation. Waves of consciousness: ongoing dynamic cortical patterns during binocular rivalry.

Dale, A.M., Sereno, M.I., 1993. Improved localization of cortical activity by combining EEG and MEG with MRI cortical surface reconstruction: a linear approach. J. Cogn. Neurosci. 5, 162–176.

David, O., Friston, K.J., in press. A neural mass model for MEG/EEG: coupling and neuronal dynamics. NeuroImage.

David, O., Garnero, L., 2002. Time-coherent expansion of MEG/EEG cortical sources. NeuroImage 17, 1277–1289.

David, O., Garnero, L., Cosmelli, D., Varela, F.J., 2002. Estimation of neural dynamics from MEG/EEG cortical current density maps: application to the reconstruction of large-scale cortical synchrony. IEEE Trans. Biomed. Eng. 49, 975–987.

David, O., Cosmelli, D., Hasboun, D., Garnero, L., 2003a. A multi-trial analysis for revealing significant corticocortical networks in magnetoencephalography and electroencephalography. NeuroImage 20 (1), 186–201.

David, O., Cosmelli, D., Lachaux, J.-P., Baillet, S., Garnero, L., Martinerie, J., 2003b. A theoretical and experimental introduction to the non-invasive study of large-scale neural phase synchronization in human beings. Int. J. Comput. Cogn. 1 (4), 53–77.

Dehaene, S., Naccache, L., 2001. Towards a cognitive neuroscience of consciousness: basic evidence and a workspace framework. Cognition 79 (1–2), 1–37.

Engel, A.K., Fries, P., Singer, W., 2001. Dynamic predictions: oscillations and synchrony in top-down processing. Nat. Rev., Neurosci. 2, 704–716.

Freeman, W.J., 1978. Models of the dynamics of neural populations. Electroencephalogr. Clin. Neurophysiol., Suppl. 34, 9–18.

Friston, K.J., 2000. The labile brain: I. Neuronal transients and nonlinear coupling. Philos. Trans. R. Soc. Lond., B Biol. Sci. 355, 215–236.

Gross, J., Kujala, J., Hamalainen, M., Timmermann, L., Schnitzler, A., Salmelin, R., 2001. Dynamic imaging of coherent sources: studying neural interactions in the human brain. Proc. Natl. Acad. Sci. U. S. A. 98, 694–699.

Halgren, E., Tommi, R., Marinkovic, K., Jousmaki, V., Hari, R., 2000. Cognitive response profile of the human fusiform area as determined by MEG. Cereb. Cortex 10, 69–81.

Hamalainen, M., Hari, R., Ilmoniemi, R., Knuutila, J., Lounasmaa, O., 1993. Magnetoencephalography. Theory, instrumentation and applications to the noninvasive study of brain function. Rev. Mod. Phys. 65, 413–497.

Haskell, E., Nykamp, D.Q., Tranchina, D., 2001. Population density methods for large-scale modeling of neuronal networks with realistic synaptic kinetics: cutting the dimension down to size. Network: Comput. Neural Syst. 12, 141–174.

Honeycutt, R.L., 1992. Stochastic Runge–Kutta algorithms: I. White noise. Phys. Rev., A 45, 600–603.

Jansen, B.H., Rit, V.G., 1995. Electroencephalogram and visual evoked potential generation in a mathematical model of coupled cortical columns. Biol. Cybern. 73, 357–366.

Kennel, M.D., Brown, R., Abarbanel, H.D.I., 1992. Determining embedding dimension for phase-space reconstruction using a geometrical construction. Phys. Rev., A 45, 3403–3411.

Kloeden, P.E., Platen, E., 1999. Numerical Solution of Stochastic Differential Equations. Springer-Verlag, Berlin, Heidelberg, New York.

Lachaux, J.-P., Rodriguez, E., Martinerie, J., Varela, F.J., 1999. Measuring phase synchrony in brain signals. Hum. Brain Mapp. 8, 194–208.

Le Van Quyen, M., Foucher, J., Lachaux, J., Rodriguez, E., Lutz, A., Martinerie, J., Varela, F.J., 2001. Comparison of Hilbert transform and wavelet methods for the analysis of neuronal synchrony. J. Neurosci. Methods 111, 83–98.

Lopes da Silva, F.H., Hoeks, A., Smits, H., Zetterberg, L.H., 1974. Model of brain rhythmic activity. The alpha-rhythm of the thalamus. Kybernetik 15, 27–37.

Lopes da Silva, F., Pijn, J.P., Boeijinga, P., 1989. Interdependence of EEG signals: linear vs. nonlinear associations and the significance of time delays and phase shifts. Brain Topogr. 2 (1/2), 9–18.

Lumer, E.D., Rees, G., 1999. Covariation of activity in visual and prefrontal cortex associated with subjective visual perception. Proc. Natl. Acad. Sci. 96 (4), 3198–3203.

Lumer, E.D., Friston, K.J., Rees, G., 1998. Neural correlates of perceptual rivalry in the human brain. Science 280, 1930–1934.

Mesulam, M.M., 1999. Spatial attention and neglect: parietal, frontal and cingulate contributions to the mental representation and attentional targeting of salient extrapersonal events. Philos. Trans. R. Soc. Lond., B Biol. Sci. 354 (1387), 1325–1346.

Mormann, F., Lehnertz, K., David, P., Elger, C.E., 2000. Mean phase coherence as a measure for phase synchronization and its application to the EEG of epilepsy patients. Physica, D 144, 358–369.

Netoff, T.I., Schiff, S.J., 2002. Decreased neuronal synchronization during experimental seizures. J. Neurosci. 22, 7297–7307.

Nunez, P.L., 1981. Electric Fields of the Brain. Oxford Univ. Press, New York.

Nunez, P.L., Srinivasan, R., Westdorp, A.F., Wijesinghe, R.S., Tucker, D.M., Silberstein, R.B., Cadusch, P.J., 1997. EEG coherency: I. Statistics, reference electrode, volume conduction, Laplacians, cortical imaging, and interpretation at multiple scales. Electroencephalogr. Clin. Neurophysiol. 103, 499–515.

Palus, M., Hoyer, D., 1998. Detecting nonlinearity and phase synchronization with surrogate data. IEEE Eng. Med. Biol. Mag. 17, 40–45.

Pereda, E., Rial, R., Gamundi, A., Gonzalez, J., 2001. Assessment of changing interdependencies between human electroencephalograms using nonlinear methods. Physica, D 148, 147–158.

Pijn, J.P., Velis, D.N., Lopes da Silva, F.H., 1992. Measurement of interhemispheric time differences in generalised spike- and -wave. Electroencephalogr. Clin. Neurophysiol. 83, 169–171.

Pikovsky, A., Rosenblum, M., Kurths, J., 2001. Synchronization. A Universal Concept in Nonlinear Sciences. Cambridge Univ. Press, Cambridge.

Prichard, D., Theiler, J., 1994. Generating surrogate data for time series with several simultaneously measured variables. Phys. Rev. Lett. 73, 951–954.

Quian Quiroga, R., Arnhold, J., Grassberger, P., 2000. Learning driver-response relationships from synchronization patterns. Phys. Rev., E 61 (5), 5142–5148.

Quian Quiroga, R., Kraskov, A., Kreuz, T., Grassberger, P., 2002. Performance of different synchronization measures in real data: a case study on electroencephalographic signals. Phys. Rev., E 65, 041903.

Rodriguez, E., George, N., Lachaux, J.P., Martinerie, J., Renault, B., Varela, F.J., 1999. Perception's shadow: long-distance synchronization of human brain activity. Nature 397, 430–433.

Rosenblum, M., Pikovsky, A., Kurths, J., 1996. Phase synchronization of chaotic oscillators. Phys. Rev. Lett. 76, 1804–1807.

Rosenstein, M.T., Collins, J.J., De Luca, C.J., 1994. Reconstruction expansion as a geometry-based framework for choosing proper delay times. Physica, D 73, 82–98.

Roulston, M.S., 1999. Estimating the errors on measured entropy and mutual information. Physica, D 125, 285–294.

Rulkov, N.F., Sushchik, M.M., Tsimring, L.S., Abarbanel, H.D., 1995. Generalized synchronization of chaos in directionally coupled chaotic systems. Phys. Rev., E 51, 980–994.

Schiff, S.J., So, P., Chang, T., Burke, R.E., Sauer, T., 1996. Detecting dynamical interdependence and generalized synchrony through mutual prediction in a neural ensemble. Phys. Rev., E 54, 6708–6724.

Sporns, O., Tononi, G., Edelman, G.M., 2000. Connectivity and complexity: the relationship between neuroanatomy and brain dynamics. Neural Netw. 13 (8–9), 909–922.

Srinivasan, R., Russell, D.P., Edelman, G.M., Tononi, G., 1999. Increased synchronization of neuromagnetic responses during conscious perception. J. Neurosci. 19, 5435–5448.

Stam, C.J., van Dijk, B.W., 2002. Synchronization likelihood: an unbiased measure of generalized synchronization in multivariate data sets. Physica, D 163, 236–251.

Stam, C.J., Pijn, J.P.M., Suffczynski, P., Lopes da Silva, F.H., 1999. Dynamics of the human alpha rhythm: evidence for non-linearity? Clin. Neurophysiol. 110, 1801–1813.

Stam, C.J., Breakspear, M., van Cappellen van Walsum, A.M., van Dijk, B.W., 2003. Nonlinear synchronization in EEG and whole-head MEG recordings of healthy subjects. Hum. Brain Mapp. 19 (2), 63–78.

Takens, F., 1981. In: Rand, D.A., Young, L.S. (Eds.), Detecting Strange Attractors in Turbulence. Springer, Berlin, p. 366.

Tallon-Baudry, C., Bertrand, O., 1999. Oscillatory gamma activity in humans and its role in object representation. Trends Cogn. Sci. 3, 151–162.

Tass, P., Wienbruch, C., Weule, J., Kurths, J., Pikovsky, A., Volkmann, J., Schnitzler, A., Freund, H.-J., 1998. Detection of *n*:*m* phase locking from noisy data: application to magnetoencephalography. Phys. Rev. Lett. 81, 3291–3294.

Theiler, J., 1986. Spurious dimension from correlation algorithms applied to limited time-series data. Phys. Rev., A 34 (3), 2427–2432.

Tong, F., 2003. Primary visual cortex and visual awareness. Nat. Rev., Neurosci. 4 (3), 219–229.

Tononi, G., Sporns, O., Edelman, G.M., 1994. A measure for brain complexity: relating functional segregation and integration in the nervous system. Proc. Natl. Acad. Sci. U. S. A. 91, 5033–5037.

Varela, F., Lachaux, J.-P., Rodriguez, E., Martinerie, J., 2001. The brainweb: phase synchronization and large-scale integration. Nat. Rev., Neurosci. 2, 229–239.

von Stein, A., Sarnthein, J., 2000. Different frequencies for different scales of cortical integration: from local gamma to long range alpha/theta synchronization. Int. J. Psychophysiol. 38, 301–313.

Wendling, F., Bellanger, J.J., Bartolomei, F., Chauvel, P., 2000. Relevance of nonlinear lumped-parameter models in the analysis of depth- EEG epileptic signals. Biol. Cybern. 83, 367–378.

Wendling, F., Bartolomei, F., Bellanger, J.J., Chauvel, P., 2001. Interpretation of interdependencies in epileptic signals using a macroscopic physiological model of the EEG. Clin. Neurophysiol. 112, 1201–1218.